ACS APPLIED MATERIALS & INTERFACES

Research Article

www.acsami.org

Improved Thermal Conductivity and Flame Retardancy in Polystyrene/Poly(vinylidene fluoride) Blends by Controlling Selective Localization and Surface Modification of SiC Nanoparticles

Jian-Ping Cao,[†] Xiaodong Zhao,[†] Jun Zhao,*[,†] Jun-Wei Zha,[†] Guo-Hua Hu,*[,‡] and Zhi-Min Dang*[,†]

[†]Department of Polymer Science and Engineering, School of Chemistry and Biological Engineering, University of Science and Technology Beijing, Beijing 100083, P. R. China

[‡]Laboratoire Réactions et Génie des Procédés, CNRS-Universté de Lorraine, UMR 7274, ENSIC, 1 rue Grandville, BP 20451, Nancy, F-54000, France

ABSTRACT: The effect of selective localization of silicon carbide (SiC) and polystyrene (PS)-coated SiC (p-SiC) nanoparticles on the thermal conductivity and flame retardancy of immiscible PS/poly(vinylidene fluoride) (PVDF) blends has been systematically studied. The scanning electron microscopy (SEM) images reveal that SiC and p-SiC nanoparticles have different selective localizations in the PS/PVDF blends. The melting and crystallization behaviors of the PVDF component investigated by using differential scanning calorimetry are consistent with the SEM results. To reduce the volume fraction of fillers in the composites, a cocontinuous structure of PS/PVDF has also been built up. The cocontinuity window for PS/PVDF blends is ~30−70 vol % according to the selective solvent dissolution technique. The selective localization of SiC in the PVDF phase of the PS/PVDF 70/30 blends produces a slightly higher thermal conductivity than that of p-SiC in the PS phase of the PS/PVDF 30/70 blends. However, the composites with selective localization of p-SiC exhibit the best combined properties of thermal conductivity and flame retardancy.

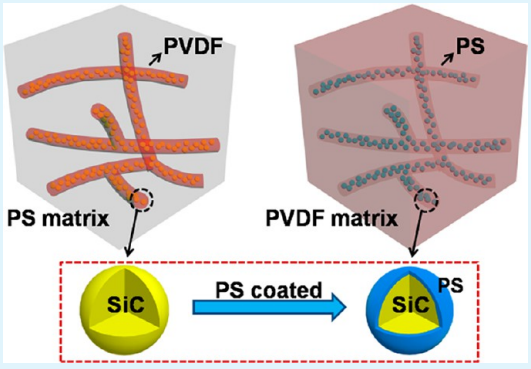

KEYWORDS: *immiscible blends, polymer nanocomposite, selective extraction, cocontinuity, cone calorimeter*

INTRODUCTION

Polymer materials represent ~20%, by weight, of electrical and electronic equipment by offering comprehensive properties that no other class of materials can give;[1] however, the continued miniaturization of electronic device components is coupled with the requirements of heat dissipation and fire safety, which requires improved thermal conductivity and enhanced flame retardancy of polymer materials.[2−5]

So far, different techniques to improve the thermal conductivity of polymeric materials have been studied. The commonly used method is to manufacture a thermally conductive composite by adding high thermal conductivity fillers. For this route, the polymer resins mainly include polystyrene (PS),[6] epoxy,[7] and polyamide 6 (PA6),[8] and the fillers could be aluminum nitride,[9] carbon nanotubes (CNTs),[10] boron nitride,[11] and carbon black (CB).[12] However, to achieve high thermal conductivity, a large amount of fillers is needed to form a well-developed conductive network, and a high volume fraction of fillers could result in poor mechanical properties, complex processing, high density, and high cost.[7,13] Very recently, a double percolation structure has been employed to improve the electrical conductivity because it can effectively reduce the volume fraction of fillers by selective localization of fillers.[14−16] Relatively few papers have reported on the use of this structure in the improvement of thermal conductivity.[17]

To achieve a double percolation structure, controlling the selective localization of the fillers is extremely crucial. There are many factors affecting the selective localization of fillers in polymer blends. Among them, two factors are generally believed to be the most important: The first is the relative viscosity of the polymer melts. In some cases, the fillers prefer to be selectively distributed in the phase with lower viscosity. This factor has been found to be the most dominant in many composites, such as polycarbonate (PC)/poly(vinylidene fluoride) (PVDF)/multiwalled carbon nanotubes,[18] poly(ethylene terephthalate) (PET)/PA6/SiO_2,[19] and poly(methy methacryate)/polypropylene/CB.[20] Therefore, tuning the viscosity of one or two phases can control the localization of the fillers in one phase or the interface between two polymer phases. The second is the surface energy of the fillers and the polymer components. Generally speaking, the dispersed phase prefers to stay in the continuous phase with the closer surface energy. The investigations on the composites of PET/polyethylene/CB,[21] PS/PA6/Fe_3O_4,[22] and acrylonitrile buta-

Received: January 23, 2013
Accepted: June 18, 2013
Published: June 18, 2013

diene styrene/PA6/CNT[23] show that which polymer phase the fillers are dominantly localized in depends on the surface energy of the fillers for the given polymer components. Thus, chemical surface modification of the fillers to change their surface energy could provide an alternative way to effectively control the selective localization.

In addition, different techniques to improve the flame-retardancy performance of polymeric materials have also been reported. The early studies on flame retardants were focused on the fire risk scenario and the development of new kinds of flame retardant additives, including organohalogen, organophosphorus, organonitrogen, and inorganic retardants.[24,25] The organohalogen retardants have good flame retardant properties, but an increase in the smoke density and the release of toxic dioxins are the problems. The organophosphorus and organonitrogen retandants must be used together, and there is an optimal ratio for effective function. For the inorganic retardants, large quantities have to be used for effective flame retardancy.[24,25] Therefore, it is necessary to generate creative ideas for developing environmentally friendly flame retardant polymeric materials.

This work deals with blends of PS and PVDF by using SiC nanoparticles as thermally conductive fillers. SiC nanoparticles have high thermal conductivity and a low coefficient of thermal expansion.[13] PVDF has excellent flame retardant properties and wide use in electrical and electronic equipment. PS has low cost, low density, and polarities different from that of PVDF. In our previous work, the SiC nanoparticles have been coated with PS successfully.[26] It was found that the PS-coated SiC (p-SiC) had better dispersion in a PS matrix than bare SiC and resulted in higher thermal conductivity of the prepared nanocomposites. This work aims to reduce the volume fraction of fillers by using the masterbatch process to control the selective localization of SiC and p-SiC nanoparticles. The different selective localization of SiC and p-SiC nanoparticles on the thermal conductivity, flame retardancy, and other important properties will be systematically investigated and discussed in detail.

EXPERIMENTAL SECTION

Materials. PS (PS-666D) pellets with a melt flow index of 8 g (10 min)$^{-1}$ and a density of 1.05 g cm^{-3} were received from Sinopec Beijing Yanshan Company (China). PVDF (PVDF-FR901) pellets with a melt flow index of 26.0 g (10 min)$^{-1}$ and a density of 1.78 g cm^{-3} were purchased from Shanghai 3F New Materials Company (China). SiC powders with a thermal conductivity of 490 W m^{-1} K^{-1} and a density of 3.2 g cm^{-3} were supplied by Hefei Kaier Nanometer Energy & Technology Co. Ltd. (China). Chloroform was purchased from the Beijing Chemical Plant (China).

Preparation of Nanocomposites. The polymers were dried at 80 °C under vacuum to remove moisture before use. The blends were prepared using a Haake mixer (Germany) at 180 °C and 100 rpm. For the preparation of PS/PVDF blends, PS and/or PVDF were mixed with SiC or p-SiC nanoparticles at various volume ratios for 15 min. The nanocomposites of PS/PVDF blends simply mixed with SiC or p-SiC nanoparticles are denoted as PS/PVDF/SiC and PS/PVDF/p-SiC. For the preparation of the selective localization of SiC or p-SiC nanoparticles in the PS/PVDF blends, the nanocomposites of PS/SiC, PS/p-SiC, PVDF/SiC, and PVDF/p-SiC were further mixed with the other polymer component in the mixer for 5 min. The prepared nanocomposites by this masterbatch process are denoted as PS-SiC/PVDF, PS-p-SiC/PVDF, PS/PVDF-SiC, and PS/PVDF-p-SiC, respectively.

Selective Extraction. The selective solvent dissolution technique is widely used and has been described in detail in the literature.[14,27−29] Samples of ∼0.2 g were immersed in a large volume of chloroform and stirred gently at room temperature to selectively extract the PS component until the samples reached a constant weight. After the dissolution process, the samples were dried in a vacuum oven at 70 °C for 8 h and then weighed again. The continuity index (CI) of PS was evaluated by the following expression:

$$CI = \frac{m_i - m_f}{w^{PS} \times m_i} \times 100\% \quad (1)$$

where m_i and m_f are the weight of the sample before and after solvent extraction and w^{PS} is the weight fraction of PS in the initial blend. When CI is equal to or above 90%, the morphology of the PS phase in the blend is considered to be continuous. It is difficult to find a solvent that can selectively dissolve PVDF without affecting the PS phase. Therefore, the PVDF phase was considered as 100% continuous when the sample was not disintegrated after the PS component had been extracted. When the sample was fragmented, the weight ratio of the biggest piece with respect to the PVDF weight in the sample before extraction was taken as the CI of the PVDF component. The reported value was the average of at least three samples with the same composition.

Morphology Characterization with Energy Dispersive Spectrometry (EDS). The morphology of the composites was observed using a Hitachi S4700 scanning electron microscope (SEM) with accelerating voltage of 20 kV. The prepared samples were fractured in liquid nitrogen, and then the fractured surface was sputtered with a thin layer of gold before SEM observation. EDS was performed on a Bruker XFlash detector 5010 to measure the relative amounts of SiC or p-SiC in the PS and PVDF phases.

Rheological Characterization. Rheological measurements of the materials were carried out at 180 °C using a MCR 502 rheometer (Anton Paar, Austria) with 25 mm parallel plate geometry. Prior to the rheological characterization, dynamic strain sweep tests were performed on all materials to determine the critical strain at which materials began to exhibit nonlinear viscoelasticity. All subsequent tests were performed at strains within the linear viscoelastic region of the materials. Small-amplitude oscillatory shear tests were performed over a frequency range of 100−0.1 rad s^{-1}.

Differential Scanning Calorimetry (DSC). DSC was performed on a DSC-60 (Shimadzu Corporation, Japan) in a nitrogen atmosphere. Temperature and enthalpy were calibrated with indium. A sample in an aluminum crucible was first heated from 30 to 200 °C at a heating rate of 10 K min^{-1} and then kept isothermal at 200 °C for 3 min to erase the thermal history. Subsequently, the sample was cooled to 30 °C at a cooling rate of 10 K min^{-1}, and then the sample was heated again to 200 °C at the same heating rate. The first cooling and second heating curves were analyzed. The degree of crystallinity (X_c) for PVDF component was calculated by the following expression:

$$X_c = \frac{\Delta H_m}{\Delta H_m^0 \times w^{PVDF}} \times 100\% \quad (2)$$

where ΔH_m is the measured value of melting enthalpy obtained during the heating process, ΔH_m^0 is the melting enthalpy of perfect PVDF crystals (104.7 J g^{-1}),[30] and w^{PVDF} is the weight fraction of PVDF in the nanocomposites.

Thermal Conductivity Measurements. The obtained nanocomposites were compression-molded into plates at 190 °C for 15 min and then at room temperature for 15 min under a pressure of 20 MPa to get a cylindrical shape with a diameter of ∼55.0 mm and thickness of ∼4.0 mm. The thermal conductivity of the nanocomposites was measured on a HC-074 heat flow meter instrument (EKO Instrument Sirading Co. Ltd., Germany) according to procedure ASTM D5470.

Flame Retardant Performance. The oxygen index (OI) and UL-94 vertical burning test were conducted according to the national standards of China GB/T2406-93 and GB4609-84, respectively. The dimensions for OI and UL-94 were 100.0 × 6.5 × 3.0 mm^3 and 125 × 13 × 3 mm^3, respectively. Flaming performance was characterized by cone calorimeter (FTT, UK) according to ISO 5660. Samples of 100 × 100 × 3 mm^3 were irradiated horizontally at a heat flux of 50 kW m^{-2}.

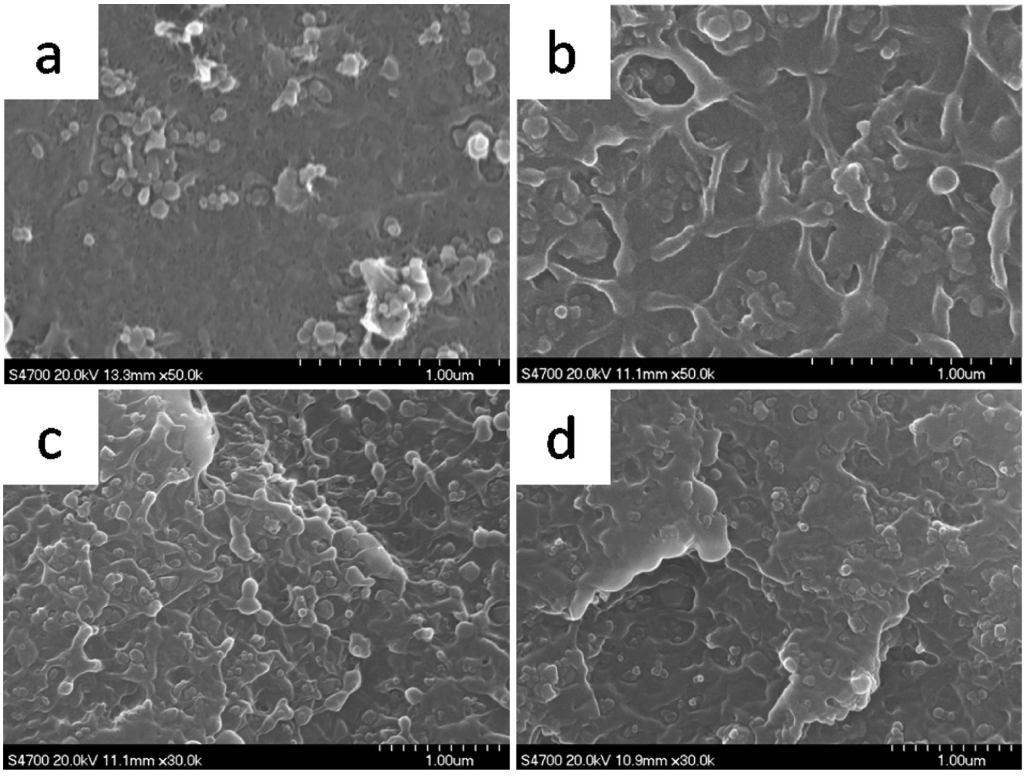

Figure 1. SEM images of (a) PS/SiC, (b) PS/p-SiC, (c) PVDF/SiC, and (d) PVDF/p-SiC nanocomposites with a filler loading of 10 vol %.

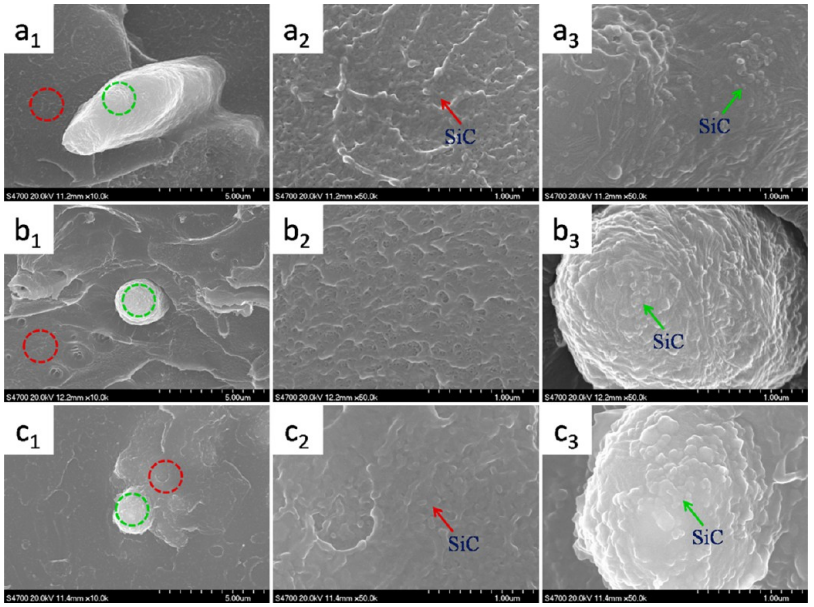

Figure 2. SEM images of SiC-filled PS/PVDF 50/50 nanocomposites with SiC loading of 4.8 vol %: (a) PS-SiC/PVDF, (b) PS/PVDF-SiC, and (c) PS/PVDF/SiC. The parts with subscripts 2 and 3 focused on the PS and PVDF phases, respectively, are the zoom-in of the red and green dashed circles, respectively, in the parts with subscript 1.

RESULTS AND DISCUSSION

The Morphology of Nanoparticles in One Polymer Component. Figure 1 shows the SEM images of PS/SiC, PS/p-SiC, PVDF/SiC, and PVDF/p-SiC nanocomposites with a filler content of 10 vol %. It can be seen that the SiC nanoparticles aggregate and protrude clearly out of the fracture surface of the PS/SiC nanocomposites. However, the sizes of the aggregates are significantly reduced, and there is a protruded network formed on the fractured surface of PS/p-SiC nanocomposites, which is a typical characteristic of ductile breakage.[31] For the PVDF nanocomposites, both SiC and p-SiC have a good dispersion in PVDF matrix, but the surface of the PVDF/SiC forms a protruded network while the PVDF/p-SiC does not. These different features can be attributed to the different interfacial interactions between the nanoparticles and the polymer matrix. The interfacial interaction between PS and p-SiC is stronger than that between PS and SiC, whereas for PVDF, it is the opposite. These different interfacial interactions

dx.doi.org/10.1021/am401703m | ACS Appl. Mater. Interfaces 2013, 5, 6915−6924

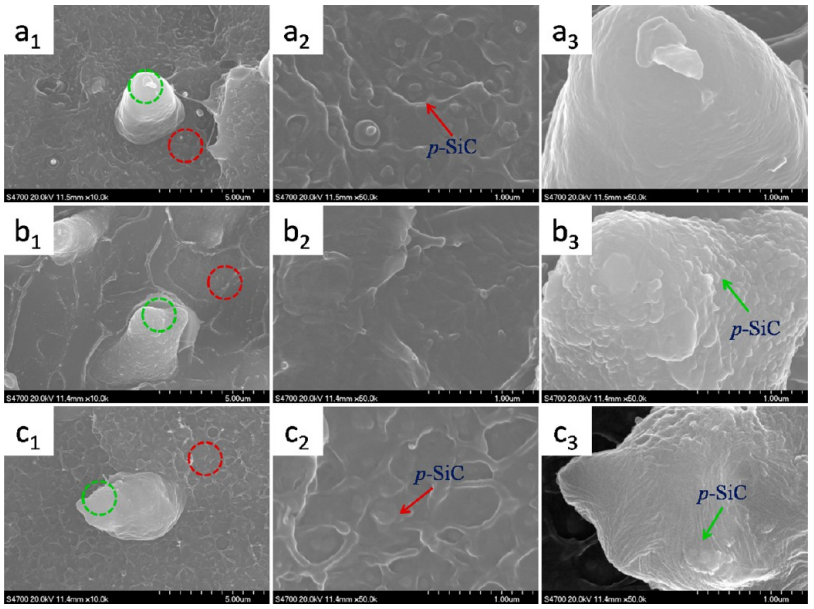

Figure 3. SEM images of p-SiC-filled PS/PVDF 50/50 nanocomposites with p-SiC loading of 4.8 vol %: (a) PS-p-SiC/PVDF, (b) PS/PVDF-p-SiC, and (c) PS/PVDF/p-SiC. The parts with subscripts 2 and 3 focused on the PS and PVDF phases, respectively, are the zoom-in of the red and green dashed circles, respectively, in the parts with subscript 1.

imply that SiC and p-SiC nanoparticles could have different locations in PS/PVDF blends.

The Selective Localizations of SiC and p-SiC Nanoparticles. To study the different localizations of SiC and p-SiC nanoparticles in PS/PVDF blends, PS/SiC, PVDF/SiC, PS/p-SiC, and PVDF/p-SiC are used as a masterbatch in this section. Figures 2 and 3 present SEM images of SiC- and p-SiC-filled PS/PVDF 50/50 nanocomposites with a filler content of 4.8 vol %. According to our previous work, the bright threadlike phase is PVDF.[32] Figure 2 clearly shows that the SiC nanoparticles are localized in both the PS and PVDF phases for the PS-SiC/PVDF and PS/PVDF/SiC nanocomposites (Figure 2a and c), but only in PVDF phase for the PS/PVDF-SiC nanocomposites (Figure 2b). For the p-SiC fillers, however, the localizations are obviously different. It can be seen from Figure 3 that the p-SiC nanoparticles are localized in the PS phase for the PS-p-SiC/PVDF nanocomposites (Figure 3a), in the PVDF phase for the PS/PVDF-p-SiC nanocomposites (Figure 3b), and mainly in the PS phase for PS/PVDF/p-SiC nanocomposites (Figure 3c).

To further determine the relative amounts of SiC or p-SiC in the PS and PVDF phases of the composites PS-SiC/PVDF, PS/PVDF/SiC, and PS/PVDF/p-SiC, the mass ratio of Si and F is measured by EDS, and the results are shown in Table 1. The filler content in PS/PVDF 50/50 nanocomposites is 4.8 vol %, so the volume fraction of SiC or p-SiC in one phase is 9.6 vol %. The mass ratio of SiC or p-SiC in the PS phase can be calculated by using 9.6 vol % minus the mass ratio of SiC or p-SiC in the PVDF phase. It can be seen from Table 1 that the SiC in the PS phase of the PS-SiC/PVDF and PS/PVDF/SiC composites is 5.84 and 3.43 vol %, respectively, whereas p-SiC in the PS phase of the PS/PVDF/p-SiC composite is 8.69 vol %. These results indicate that SiC prefers to stay in the PVDF phase and p-SiC prefers PS phase.

By comparing Figure 2a and b, it is clear that the SiC nanoparticles can diffuse from the PS phase to the PVDF phase, but the reverse cannot happen. The reason for the diffusion of SiC nanoparticles from PS to PVDF is that the interfacial

Table 1. The Relative Amounts of SiC or p-SiC in the PS or PVDF Phases in Composites of PS-SiC/PVDF, PS/PVDF/SiC, and PS/PVDF/p-SiC Measured by EDS[a]

samples	m_{Si}/m_F (%)	m_{SiC}/m_{PVDF} (%)	v_{SiC}/v_{PVDF} (%)	v_{SiC}/v_{PS} (%)
PS-SiC/PVDF	7.97 ± 0.49	6.76 ± 0.41	3.76 ± 0.20	5.84 ± 0.20
PS/PVDF/SiC	13.08 ± 0.43	11.10 ± 0.36	6.17 ± 0.23	3.43 ± 0.23
PS/PVDF/p-SiC	1.92 ± 0.11	1.63 ± 0.01	0.91 ± 0.05	8.69 ± 0.05

[a] m_{Si}, m_F, m_{SiC}, m_{PVDF}, v_{SiC}, v_{PVDF}, and v_{PS} denote the mass of Si, F, and SiC, and volume of SiC, PVDF, and PS, respectively.

interaction between SiC and PVDF is stronger than that between SiC and PS. For the PS/PVDF-SiC composites, however, there is a factor other than the interfacial interaction: the viscosity of PVDF and PS. As shown in Figure 4, the complex viscosity (η^*) of both PVDF and PS decreases with

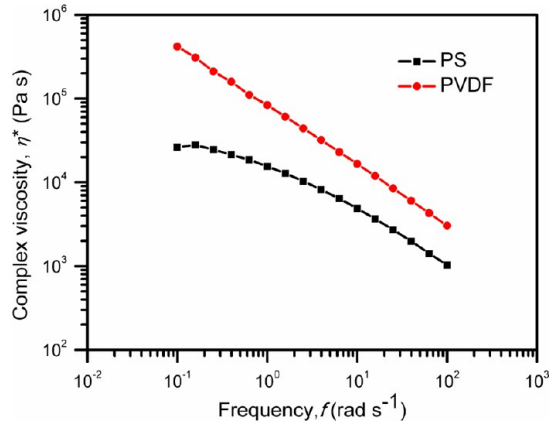

Figure 4. η^* as a function of frequency at 180 °C for PS and PVDF.

dx.doi.org/10.1021/am401703m | ACS Appl. Mater. Interfaces 2013, 5, 6915−6924

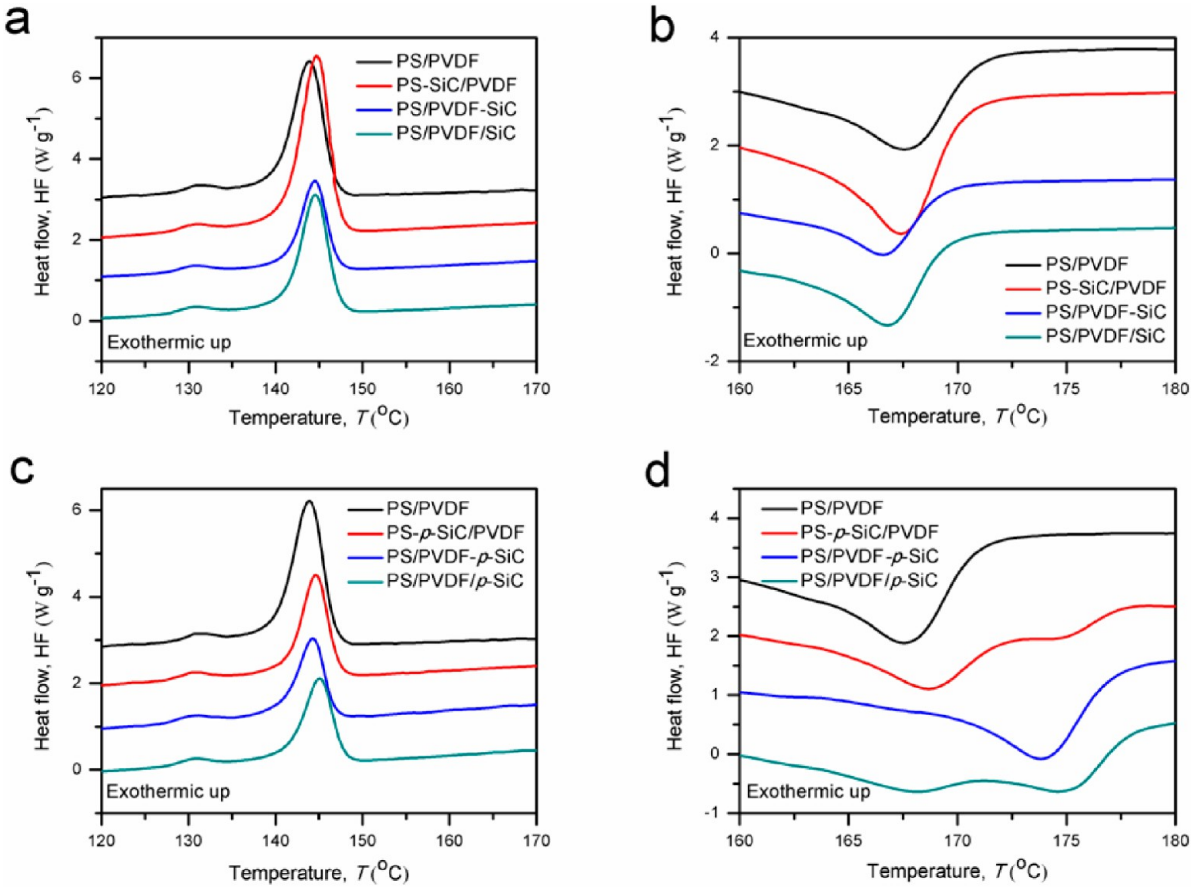

Figure 5. DSC curves of (a, b) SiC- and (c, d) p-SiC-filled PS/PVDF 50/50 nanocomposites with filler content of 4.8 vol %: (a, c) cooling and (b, d) heating.

increasing frequency from 10^{-1} to 10^{2} rad s^{-1} at 180 °C, and the η^* of PVDF is always higher than that of PS. That is to say, the viscosity of PVDF is higher than that of PS for the mixing process. Therefore, the dissipative energy for the diffusion of SiC nanoparticles from PVDF to PS is high, and the transfer can hardly be observed within 5 min, as used in our experiments. In contrast, for the p-SiC-filled PS/PVDF nanocomposites, the nanoparticles could never diffuse from one phase to another phase (as shown in Figure 3a and b). The reason might be that the PS coating of p-SiC changes the surface energy of SiC nanoparticles and the interfacial interaction between p-SiC and PS is stronger than that between p-SiC and PVDF. Therefore, the p-SiC nanoparticles prefer to localize in the PS phase and do not diffuse from the PS phase to the PVDF phase.

It is interesting to find that the p-SiC nanoparticles can be fixed in the PS phase (Figure 3c), but the SiC cannot (Figure 2c). There might be two reasons. First, because of the kinetic reason, the nanoparticles prefer to selectively stay in the phase with the lower melt viscosity in a multiphase blend, that is, the PS phase in our system. Second, there might be some functional polar groups, such as carboxyl and hydroxyl, on the surface of the SiC nanoparticles. For the PS/PVDF blends, PVDF has a higher polarity than PS. Therefore, the interaction between SiC and PVDF is stronger than that between SiC and PS, and SiC prefers to stay with PVDF rather than with PS. For p-SiC, the surface of SiC is covered by PS. Therefore, p-SiC prefers to stay in the PS phase of PS/PVDF blends. On the basis of the consideration of these factors, the observed distribution of SiC and p-SiC nanoparticles in the PS/PVDF blends as shown in Figures 2 and 3 is actually a compromise of these two competing factors.

As is well-known, the nanoparticles are widely used as a nucleating agent for polymer crystallization. Thus, the selective distribution of SiC and p-SiC in the nanocomposites can be further confirmed by examining the crystallization and melting behaviors of the components. Figure 5 shows the crystallization and melting behaviors of PS/PVDF 50/50 blends with 4.8 vol % SiC or p-SiC nanoparticles by different processing conditions. The obtained data are shown in Table 2. As shown in Table 2, PVDF in the PS/PVDF blends has a crystallization temperature (T_c) and a melting temperature

Table 2. Melting and Crystallization Data of SiC- and p-SiC-Filled PS/PVDF Nanocomposites with Different Processing Conditions[a]

samples	T_c (°C)	T_{m1} (°C)	T_{m2} (°C)	X_c (%)
PS/PVDF	143.8	167.6		39.5
PS-SiC/PVDF	144.7	167.4		53.7
PS/PVDF-SiC	144.6	166.8		21.5
PS/PVDF/SiC	144.5	166.6		39.6
PS-p-SiC/PVDF	144.6	168.6	174.8	43.3
PS/PVDF-p-SiC	144.3		173.8	21.4
PS/PVDF/p-SiC	145.1	168.2	175.0	41.1

[a]The data are obtained from the DSC measurements in Figure 5. [b]T_{m1}, lower melting temperature; T_{m2}, higher melting temperature.

dx.doi.org/10.1021/am401703m | ACS Appl. Mater. Interfaces 2013, 5, 6915−6924

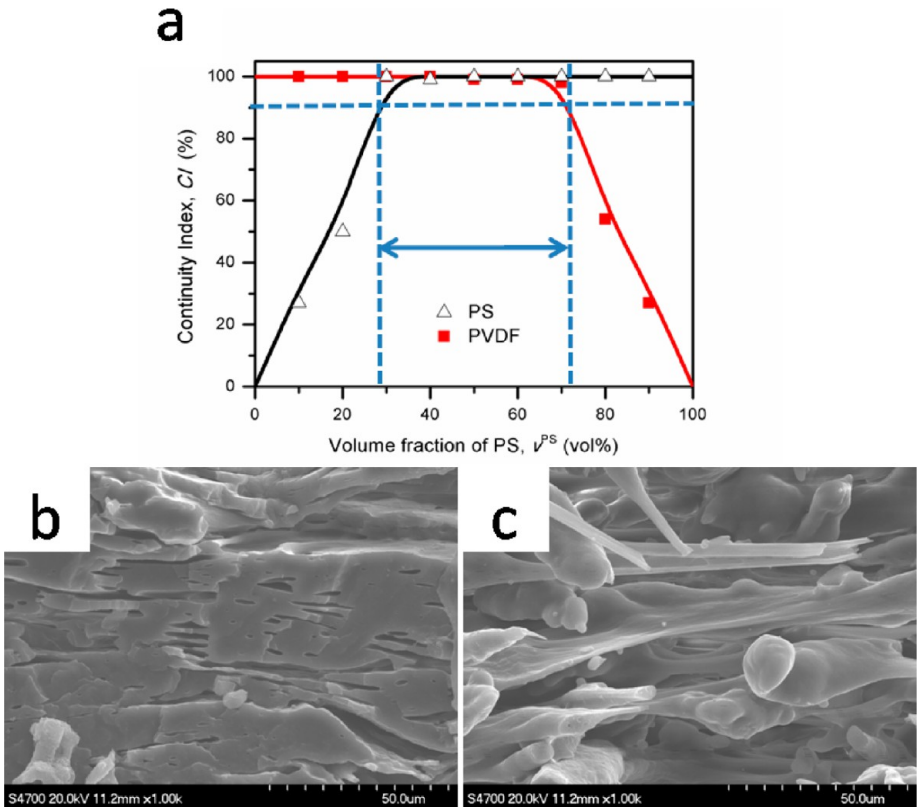

Figure 6. (a) Continuity index of both components in PS/PVDF blends and (b, c) SEM images of fractured surface of PS/PVDF 30/70 and 70/30 blends, respectively. The horizontal and vertical dashed lines coupled with the double-arrow solid line indicate the cocontinuity window of the PS/PVDF blend. PS is already extracted by chloroform. The solid lines in part a are a guide to the eyes.

(T_m) of 143.8 and 167.6 °C, respectively. As shown in Figure 5 and Table 2, the T_c of PVDF in all composites shifts slightly to higher temperatures, which can be attributed to the heterogeneous nucleation effect of nanoparticles for PVDF crystallization. The T_m of PVDF shifts to lower temperatures for SiC-filled nanocomposites, whereas for the nanocomposites of p-SiC, there are two melting peaks for the PS-p-SiC/PVDF and PS/PVDF/p-SiC nanocomposites.

The T_m of PS/PVDF-p-SiC nanocomposite is 173.8 °C, which is much higher than other nanocomposites. It is because PVDF suggests dual melting endotherms for each thermogram which is called reorganization.[33] The lower temperature peak represents the melting of the original metastable crystallites formed at the crystallization temperature from the amorphous phase, and the upper temperature peak corresponds to the melting of the crystallites recrystallized and perfected during the heating process. In the DSC trace of the p-SiC-filled PS/PVDF nanocomposites, the peak is at ~168 °C, and the high-temperature peak is at ~174 °C. The melting peak at 174 °C is proved to be the melting of the α-conformation, so the two melting peaks in the samples mean only α-conformation, not the transition of α-conformation to β-conformation, which varies between 190 and 300 °C.[34] This result indicates that the p-SiC can defer the crystallization rate of PVDF. It is very interesting that the two melting peaks for the PS/PVDF/p-SiC nanocomposite look like the superposition of the larger peak of PS-p-SiC/PVDF nanocomposite and the peak of PS/PVDF-p-SiC nanocomposite, which is consistent with the selective distribution of p-SiC nanoparticles in three different nanocomposites.

It is interesting to notice that the degree of crystallinity (X_c) also depends on the selective localizations of the nanoparticles, as shown in Figure 5 and Table 2. When only a small amount of nanoparticles is localized in the PVDF phase, as is the case in the nanocomposites of PS-SiC/PVDF, PS-p-SiC/PVDF, and PS/PVDF/p-SiC, the X_c will be increased. In contrast, if the nanoparticles are all in the PVDF phase, as is the case in the nanocomposites of PS/PVDF-SiC, PS/PVDF/SiC, and PS/PVDF-p-SiC, the X_c will be decreased. The main reason might be that a small amount of nanoparticles in the PVDF phase exhibits an effective nucleation effect and increases the X_c, whereas a large amount of nanoparticles (up to 10 vol %) in the PVDF phase causes restriction to the mobility and diffusion of polymer chain segments and hinders the crystallization.

Cocontinuity Study of PS/PVDF Blends. Figure 6a presents the phase continuity index of both components in PS/PVDF blends measured by selective solvent extraction. It can be clearly seen that the cocontinuity window for PS/PVDF blends is ~30−70 vol %. Figure 6b and c shows the SEM micrographs of the fractured surface of PS/PVDF blends with a volume ratio of 30/70 and 70/30, respectively. The PS phase was already extracted by chloroform to clarify the morphology. Two different phase morphologies are distinguishable in Figure 6b and c: the blend with 30 vol % PS consists of PS dispersed in the PVDF matrix and the PS phase is the interconnected thread, whereas the blend with 70 vol % PS is the opposite.

The double percolation technique is one method that can significantly reduce the percolation threshold in composites. When particles are added into a blend with two polymer components, the fillers could be selectively dispersed in one phase or accumulated at the interface because of their different

interfacial interaction to the polymer components. To produce highly thermal conductive composites containing a low content of filler, the continuous structure of the filled phase is necessary. In other words, the filled phase should form the matrix of a dispersed blend or exhibit a continuous phase in a cocontinuous blend. For this purpose, the volume ratio of PS/PVDF was selected to be 30/70 when the nanoparticles were distributed in the PS phase, and the volume ratio of PS/PVDF was selected to be 70/30 when the nanoparticles were localized in the PVDF phase.

The Thermal Conductivity and Flame Retardancy of the Composites. Because SiC can fully locate in the PVDF phase and p-SiC prefers to locate in PS phase, the volume ratio of PS/PVDF is selected to be 70/30 for SiC-filled PS/PVDF composites, but it is 30/70 for p-SiC-filled PS/PVDF composites. Figure 7 shows the effect of the volume fraction

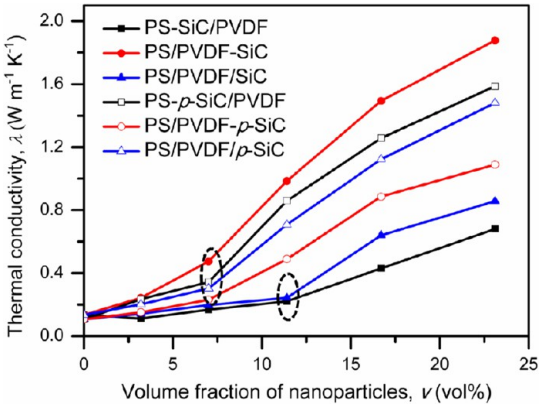

Figure 7. Effect of the volume fraction of SiC and p-SiC fillers on the thermal conductivity of their PS/PVDF composites with different processing conditions. The lines are a guide to the eyes. The dashed circles indicate the percolation thresholds.

of SiC and p-SiC fillers on the thermal conductivity of their PS/PVDF composites. It can be seen that the thermal conductivity increases with increasing filler content. The thermal conductivity of PS-SiC/PVDF and PS/PVDF/SiC shows a slight increase, whereas the other four kinds of composites increase remarkably. When the filler content is below 7.0 vol %, the thermal conductivity of PS/PVDF-SiC, PS-p-SiC/PVDF, and PS/PVDF/p-SiC increases relatively less remarkably because the nanoparticles cannot contact each other. However, with further increasing filler content, the nanoparticles begin to contact each other and gradually form a three-dimensional heat conduction network. The percolation threshold of nanoparticles is ~13 vol % for the nanocomposites of PS-SiC/PVDF and PS/PVDF/SiC; it is ~8 vol % for the other four nanocomposites.

The thermal conductivity of PS/PVDF 70/30 (0.107 W m^{-1} K^{-1}) is lower than that of PS/PVDF 30/70 (0.135 W m^{-1} K^{-1}). When the filler content is 23.1 vol %, the thermal conductivity of PS-SiC/PVDF, PS/PVDF-SiC, PS/PVDF/SiC, PS-p-SiC/PVDF, PS/PVDF-p-SiC, and PS/PVDF/p-SiC increases to 0.68, 1.88, 0.86, 1.59, 1.08, and 1.48 W m^{-1} K^{-1}, respectively, which are all much higher than the PS/PVDF blends. The amount of the added filler has been greatly reduced compared with the other literature.[35−38]

It can also be seen from Figure 7 that for the same filler content, the PS-SiC/PVDF and PS/PVDF/SiC have lower thermal conductivity. It is because the SiC is distributed throughout both phases (based in Figure 2) that there are no well-formed thermal paths for enhanced conduction. To better understand this result, an illustration is proposed in Figure 8a.

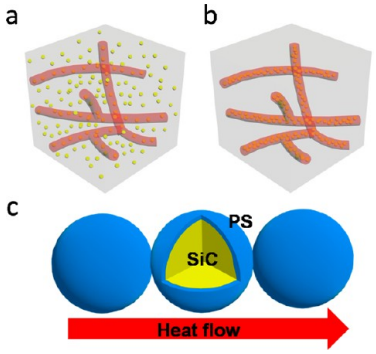

Figure 8. Illustration of (a) uniform dispersion of the nanoparticles in the PS/PVDF blends, (b) the nanoparticles dispersed in one phase, and (c) heat flow between p-SiC nanoparticles.

When the nanoparticles are uniformly dispersed in the PS/PVDF blend without selective localization, it is difficult for the nanoparticles to form thermal conducting paths by contact of the thermal conductive nanoparticles because of the low local concentration. The thermal conductivity of PS/PVDF/SiC is a little higher than PS-SiC/PVDF, with filler content more than 11.4 vol % because more SiC locates in the PVDF phase in the PS/PVDF 70/30 blend to form thermal paths (Table 1). The results for PS/PVDF-SiC are also quite clear: in this sample, SiC strongly localizes in PVDF rather than PS (Figure 2b), the thermal conducting paths by overlapping of the nanoparticles become easier because the content of SiC in the PVDF phase is very high. For example, when the content of SiC is 23.1 vol % in PS/PVDF 70/30, it is equal to 50 vol % in the PVDF phase. Although the PVDF phase is not quite fully continuous (Figure 6), there is still strong enhancement of the thermal conductivity due to the mechanism illustrated in Figure 8b.

For the p-SiC-filled PS/PVDF 30/70 composites, the thermal conductivity of PS-p-SiC/PVDF is a little higher than PS/PVDF/p-SiC because p-SiC can fully locate in the PS phase (Figure 3) to form thermal conductive paths. Although p-SiC can selectively localize in the PVDF phase in the PS/PVDF-p-SiC composite, the thermal conductive paths are fewer than PS-p-SiC/PVDF and PS/PVDF/p-SiC because of the larger proportion of PVDF in the PS/PVDF 30/70 blend. Therefore, a different localization of nanoparticles could result in a different thermal conductivity of the nanocomposites. It can also be seen from Figure 7 that the thermal conductivity of the PS/PVDF-SiC nanocomposite is a little higher than that of PS-p-SiC/PVDF. The reason is that when the p-SiC nanoparticles are dispersed in PS phase and connect to each other to form a thermally conductive network, the coating of PS on the surface of SiC acts as a barrier to heat transmission (Figure 8c). In summary, the thermal conductivity follows the sequence of PS-SiC/PVDF < PS/PVDF/SiC < PS/PVDF-p-SiC < PS/PVDF/p-SiC < PS-p-SiC/PVDF < PS/PVDF-SiC.

Agari's model presents a relationship between the thermal conductivity of composites and the volume fractions of filler, which is also dependent on the state of dispersion and the structure of the matrix.[39] The model of Agari considered the effect of dispersion state by introducing factors C_1 and C_2:

$$\log \lambda_c = \nu_f C_2 \log \lambda_f + (1 - \nu_f) \log(C_1 \lambda_m) \quad (3)$$

dx.doi.org/10.1021/am401703m | ACS Appl. Mater. Interfaces 2013, 5, 6915−6924

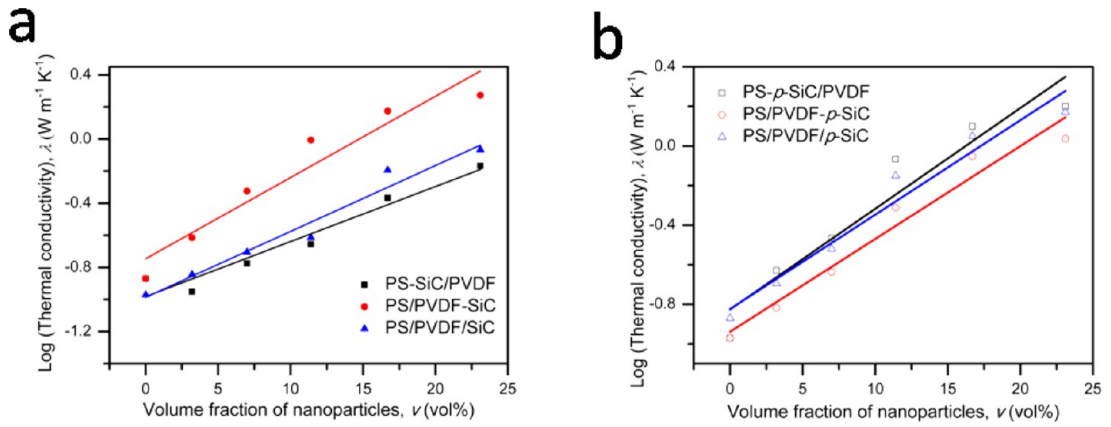

Figure 9. Comparison of the thermal conductivity of (a) SiC- and (b) p-SiC-filled PS/PVDF 70/30 composites with Agari's model.

where V_f is the volume fraction of filler; λ_c, the thermal conductivity of composite; λ_f, the thermal conductivity of filler; λ_m, the thermal conductivity of matrix; C_1 is a factor relating to the structure of the polymer; and C_2 is a factor relating to the ease in forming conductive chains of the filler.

For further probing the effect of selective localization of filler on the ease in forming conductive paths, the thermal conductivity of SiC- and p-SiC-filled PS/PVDF 70/30 by different processing conditions and Agari's model were selected. As shown in Figure 9, thermal conductivity of the composites follows Agari's model well. Through data fitting, C_1 and C_2 for the SiC- and p-SiC-filled PS/PVDF composites are obtained and shown in Table 3. For the SiC-filled PS/PVDF 70/30 composites, C_1 has little difference between composites of PS-SiC/PVDF and PS/PVDF/SiC, but it is higher in the composite of PS/PVDF-SiC because the SiC's being fully dispersed in the PVDF phase affects the structure of the PVDF phase. The C_2 of the composite of PS/PVDF-SiC is the highest, which means the formation of thermal conductive paths with selective localization of fillers in PS/PVDF is more likely. C_1 and C_2 are also affected by the selective localization of p-SiC in the PS/PVDF 30/70 blend. C_1 and C_2 are higher when all or mostly p-SiC nanoparticles are diapered in the PS phase to affect the structure and form the thermal conductive paths, such as the composites of PS-p-SiC/PVDF and PS/PVDF/p-SiC.

Table 3. C_1 and C_2 for Agari's Model for SiC- and p-SiC-Filled PS/PVDF Blends

samples	C_1	C_2
PS-SiC/PVDF	0.773	−0.352
PS/PVDF-SiC	1.329	−0.259
PS/PVDF/SiC	0.765	−0.351
PS-p-SiC/PVDF	1.395	−0.229
PS/PVDF-p-SiC	1.076	−0.332
PS/PVDF/p-SiC	1.403	−0.288

OI is an important parameter for evaluating the ease of extinguishment of polymeric materials under the same conditions. It denotes the lowest volume concentration of oxygen that will sustain candle burning when the material is mixed with nitrogen and oxygen. Therefore, the higher the OI is, the better the flame retardancy of the composites.

The set of UL-94 V tests is also commonly used to measure the ignitability and flame-spread of vertical bulk materials exposed to a small flame. It is classified as V-0, V-1, or V-2 according to the length of the combustion time by GB4609-84. The effect of filler content on the OI values and UL-94 results of PS/PVDF composites with different processing conditions are shown in Figure 10 and Table 4. It can be seen from Figure 10 that the OI of SiC-filled PS/PVDF 70/30 composites is lower than that of p-SiC-filled PS/PVDF 30/70 composites with the same filler content. The reason is that the OI of PVDF is 47%, but the OI of PS is only 18%. Therefore, the OI of the PS/PVDF 70/30 blend is much lower than that of the PS/PVDF 30/70 blend.

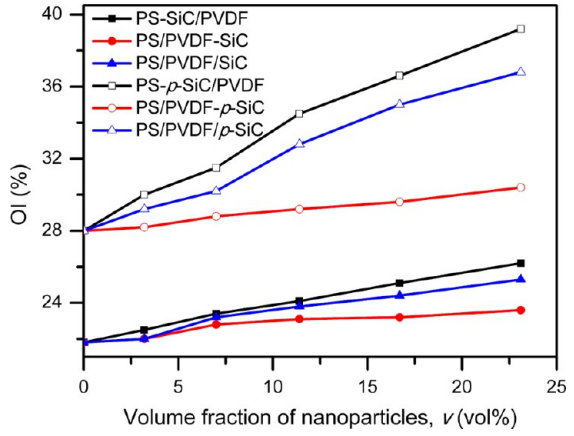

Figure 10. Effect of the volume fraction of SiC and p-SiC fillers on the OI of their PS/PVDF composites under different processing conditions. The lines are a guide to the eye.

Table 4. Effect of Filler Content on the UL-94 Rating of SiC- and p-SiC-Filled PS/PVDF Nanocomposites under Different Processing Conditions

vol faction SiC (vol %)	PS-SiC/PVDF	PS/PVDF-SiC	PS/PVDF/SiC	PS-p-SiC/PVDF	PS/PVDF-p-SiC	PS/PVDF/p-SiC
0	NR[a]	NR	NR	V-1	V-1	V-1
3.2	NR	NR	NR	V-0	V-1	V-0
7.0	NR	NR	NR	V-0	V-1	V-0
11.4	NR	NR	NR	V-0	V-1	V-0
16.7	NR	NR	NR	V-0	V-1	V-0
23.1	V-2	NR	NR	V-0	V-1	V-0

[a]NR: no UL-94 rating.

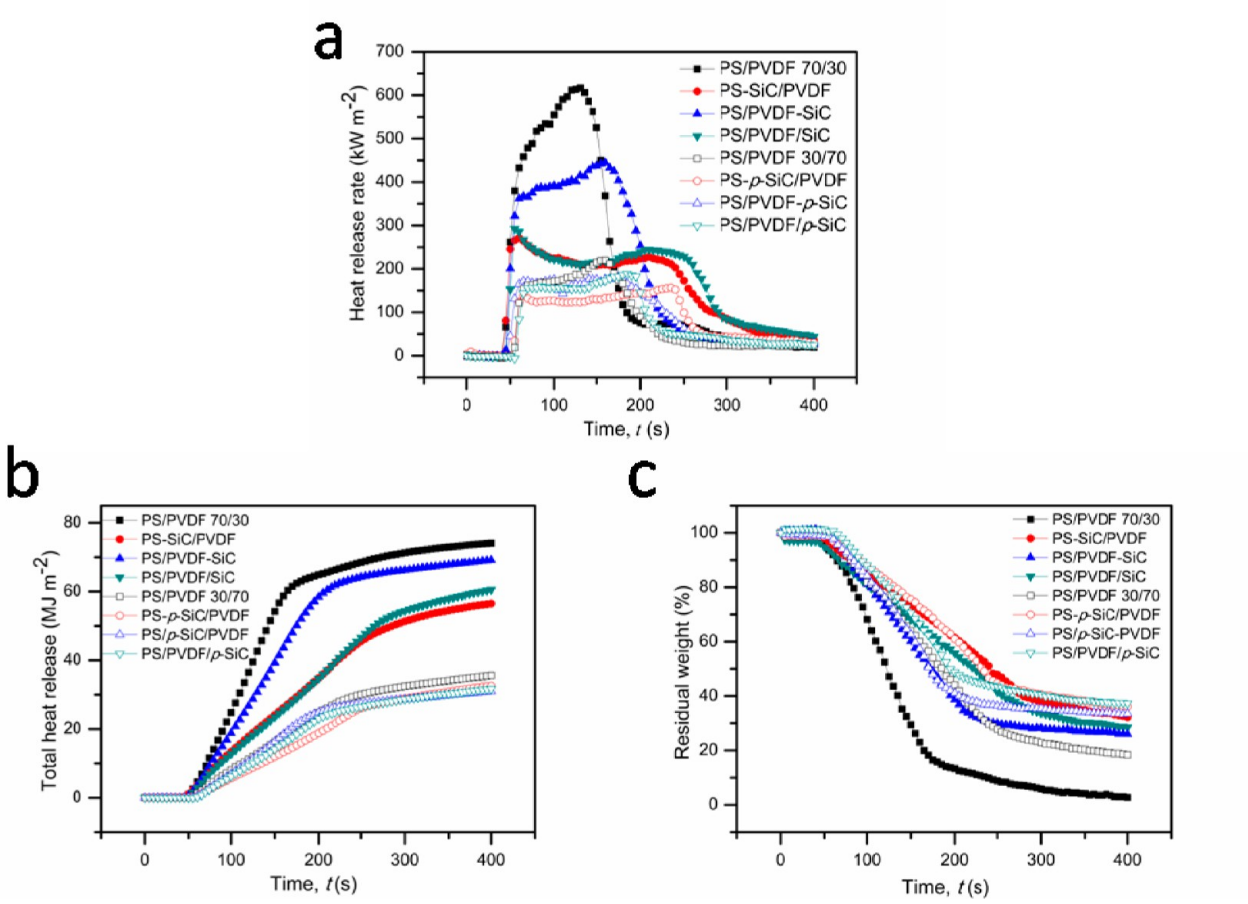

Figure 11. Effect of different processing on cone calorimeter results (a) HRR, (b) THR, and (c) MLR of SiC- and p-SiC-filled PS/PVDF composites with 11.4 vol % filler content.

For the SiC-filled PS/PVDF 70/30 composites, the OI increases slightly and only PS-SiC/PVDF with 23.1 vol % filler content passes the UL-94 V-2 for the SiC-filled PS/PVDF 70/30 composites. The OI of PS/PVDF-SiC is the lowest because the SiC is fully located in PVDF phase (Figure 2b), which cannot increase the flame retardancy of PS phase with poor flame retardant properties, resulting in the low OI of the whole composites. When some SiC nanoparticles are dispersed in PS phase, the OI is improved like the composites of PS/PVDF/SiC and PS-SiC/PVDF. The OI of PS-SiC/PVDF is a little higher than the PS/PVDF/SiC because more SiC is dispersed in PS phase (Table 1). Therefore, the order of OI of the nanocomposites follows PS/PVDF-SiC < PS/PVDF/SiC < PS-SiC/PVDF for the same filler content, which is different from the thermal conductivity order. While for the p-SiC-filled PS/PVDF 30/70 nanocomposites, the OI increases remarkably with the increase of p-SiC content and all the composites pass the UL-94 rating for the composites of PS-p-SiC/PVDF/SiC and PS/PVDF/p-SiC, because all p-SiC nanoparticles are dispersed in PS phase for the composite of PS-p-SiC/PVDF/SiC and only a little in PVDF phase for the composite of PS/PVDF/p-SiC. However, for the composite of PS/PVDF-p-SiC, all p-SiC nanoparticles locate in PVDF phase, resulting in the slight OI increase and the UL-94 rating does not change with the increase of p-SiC. Therefore, by keeping PVDF as the major phase of the PS/PVDF blends and selectively localizing SiC or p-SiC in the PS phase, we can greatly improve the flame retardancy of the composites.

Cone calorimeter is also an effective approach to evaluate the combustion behavior of materials. A wealth of information on the combustion behavior can be obtained from the test. For instance, the heat release rate (HRR), total heat release (THR) and mass loss rate (MLR) are important parameters and can be used to evaluate the intensity, developing and spreading degree of fires. Figure 11 shows the plots of SiC- and p-SiC-filled PS/PVDF composites with 11.4 vol % filler content by different processing, which is derived from cone calorimeter tests at a heat flux of 50 kW m^{-2}. It can be seen from Figure 11a that the blend of PS/PVDF 70/30 is burnt out within 140 s after ignition and reaches a maximum HRR value of 617 kW m^{-2} at 130 s. While for the blend of PS/PVDF 30/70, the burnt out time is 170 s after ignition and the PHRR is 220 kW m^{-2} at 160 s, which can be attribute to the excellent flame retardantcy of PVDF. The addition of SiC or p-SiC in PS/PVDF blend can not only significantly decrease the PHRR and HRR but also prolong the combustion time of the composites. Furthermore, when the SiC or p-SiC is mixed with PS in advance, the HRR is lower than by other processing. Because the integrity and strength of carbonaceous char layers of PS phase can be reinforced by the addition of SiC or p-SiC, which consequently improve the flame retardant properties of the whole material.

Figure 11b and c shows the THR and MLR curves of SiC- or p-SiC-filled PS/PVDF composites with 11.4 vol % filler content, respectively. A similar conclusion can be drawn that the THR and MLR are decreased with the incorporation of SiC or p-SiC of PS/PVDF composites. As shown in Figure 11b, the

THR curve of the PS/PVDF 70/30 blend reaches its maximum value of 74 MJ m^{-2} at 400 s, whereas the value is only 41 MJ m^{-2} for PS/PVDF 30/70 for the same time. Moreover, when the SiC or p-SiC is mixed with PVDF in advance, the THR value is higher than other composites mixed by other processing means, which is consistent with the HRR results. In addition, PS/PVDF 30/70 shows a significantly lower MLR than PS/PVDF 70/30, and the higher the filler content in the PS phase, the lower MLR is. After combustion, the char residue of PS-SiC/PVDF and PS-p-SiC/PVDF is higher than other processing with the same component. It indicates that according to the localization of SiC or p-SiC in the PS phase, much more char residue of the composites forms, which prevents the inner matrix from further degradation.

CONCLUSIONS

The thermal conductivity and flame retardancy of immiscible PS/PVDF blends by selectively localizing SiC nanoparticles in different phases have been studied. The selective localization of SiC nanoparticles was achieved by using surface modification of SiC and the masterbatch process. The selective localization of SiC nanoparticles in the PVDF phase with a PS/PVDF volume ratio of 70/30 produced higher thermal conductivity than did p-SiC in the PS phase with a PS/PVDF volume ratio of 30/70. However, the selective localization of p-SiC in the PS phase exhibited much better flame retardant properties than did SiC in the PVDF phase. The composites with selective locations of p-SiC exhibited excellent combined properties of thermal conduction and flame retardancy because the p-SiC nanoparticles were selectively localized in the PS phase, and the PVDF phase was a flame retardant matrix. Therefore, it is possible to obtain a flame-retardant composite with high thermal conductivity by selectively locating the fillers with high thermal conductivity in the flammable phase.

AUTHOR INFORMATION

Corresponding Author

*E-mail: (J.Z.) junzhao@ustb.edu.cn, (Z.-M.D.) dangzm@ustb.edu.cn, (G.-H.H.) guo-hua.hu@univ-lorraine.fr.

Notes

The authors declare no competing financial interest.

ACKNOWLEDGMENTS

This work was financially supported by the NSF of China (Grant Nos. 51073015 and 51207009), Beijing Municipal Excellent Scholars (2011D009006000005), and the State Key Laboratory of Power Transmission Equipment and System Security (No.2007DA10512712406) at Chongqing University. The authors also acknowledge Prof. Dr. Fenghua Chen of the Institute of Chemistry, Chinese Academy of Sciences for her assistance in rheological measurements.

REFERENCES

(1) Dawson, R. B.; Landry, S. D. IEEE Symposium on Electroinics and the Environment: New York, May 10–13, 2004; pp 46–50.
(2) Yu, A.; Ramesh, P.; Itkis, M. E.; Bekyarova, E.; Haddon, R. C. *J. Phys.Chem. C* **2007**, *111*, 7565–7569.
(3) Dawson, R. B.; Landry, S. D.; Ranken, P. F.; Yamada, H. IEEE 3rd International Symposium on Environmentally Conscious Design and Inverse Manufacturing: Tokyo, December 8–11, 2003, pp 792–798.
(4) Lin, W.; Moon, K. S.; Wong, C. P. *Adv. Mater.* **2009**, *21*, 2421–2424.
(5) Sain, M.; Park, S. H.; Suhara, F.; Law, S. *Polym. Degrad. Stab.* **2004**, *83*, 363–367.
(6) Yu, S.; Hing, P.; Hu, X. *Composites, Part A* **2002**, *33*, 289–292.
(7) Im, H.; Kim, J. *Carbon* **2011**, *49*, 3503–3511.
(8) Kim, S. R.; Poostforush, M.; Kim, J. H.; Lee, S. G. *Express Polym. Lett.* **2012**, *6*, 476–484.
(9) Shi, Z.; Radwan, M.; Kirihara, S.; Miyamoto, Y.; Jin, Z. *Appl. Phys. Lett.* **2009**, *95*, 2241041–2241043.
(10) Zhou, T.; Wang, X.; Liu, X. H.; Lai, J. Z. *Express Polym. Lett.* **2010**, *4*, 217–226.
(11) Li, T. L.; Hsu, S. L. C. *J. Phys. Chem. B* **2010**, *114*, 6825–6829.
(12) Song, J.; He, Y.; Ma, L. *Adv. Mater. Res.* **2011**, *221*, 466–471.
(13) Zhou, T.; Wang, X.; Liu, X.; Xiong, D. *Carbon* **2010**, *48*, 1171–1176.
(14) Al-Saleh, M. H.; Sundararaj, U. *Eur. Polym. J.* **2008**, *44*, 1931–1939.
(15) Pang, H.; Chen, C.; Bao, Y.; Chen, J.; Ji, X.; Lei, J.; Li, Z. M. *Mater. Lett.* **2012**, *79*, 96–99.
(16) Gao, X.; Zhang, S.; Mai, F.; Lin, L.; Deng, Y.; Deng, H.; Fu, Q. *J. Mater. Chem.* **2011**, *21*, 6401–6408.
(17) Yorifuji, D.; Ando, S. *J. Mater. Chem.* **2011**, *21*, 4402–4407.
(18) Su, C.; Xu, L.; Zhang, C.; Zhu, J. *Compos. Sci. Technol.* **2011**, *71*, 1016–1021.
(19) Qu, C.; Yang, H.; Liang, D.; Cao, W.; Fu, Q. *J. Appl. Polym. Sci.* **2007**, *104*, 2288–2296.
(20) Feng, J.; Chan, C.; Li, J. *Polym. Eng. Sci.* **2003**, *43*, 1058–1063.
(21) Dai, K.; Li, Z. M.; Xu, X. B. *Polymer* **2008**, *49*, 1037–1048.
(22) Wu, G.; Cai, X.; Lin, X.; Yui, H. *React. Funct. Polym.* **2010**, *70*, 732–737.
(23) Meincke, O.; Kaempfer, D.; Weickmann, H.; Friedrich, C.; Vathauer, M.; Warth, H. *Polymer* **2004**, *45*, 739–748.
(24) Konnicke, D.; Kuhn, A.; Mahrholz, T.; Sinapius, M. *J. Mater. Sci.* **2011**, *46*, 7046–7055.
(25) Laoutid, F.; Bonnaud, L.; Alexandre, M.; Lopez-Cuesta, J. M.; Dubois, P. *Mater. Sci. Eng., R* **2009**, *63*, 100–125.
(26) Cao, J. P.; Zhao, J.; Zhao, X.; Dang, Z. M.; Hu, G. H. *J. Appl. Polym. Sci.* **2013**, DOI: 10.1002/app.39186.
(27) Lu, C.; Hu, X. N.; He, Y. X.; Huang, X.; Liu, J. C.; Zhang, Y. Q. *Polym. Bull.* **2012**, *68*, 2071–2087.
(28) Martin, G.; Barres, C.; Sonntag, P.; Garois, N.; Cassagnau, P. *Mater. Chem. Phys.* **2009**, *113*, 889–898.
(29) Wang, L.; Guo, Z. X.; Yu, J. *J. Appl. Polym. Sci.* **2012**, *123*, 1218–1226.
(30) Marega, C.; Marigo, A. *Eur. Polym. J.* **2003**, *39*, 1713–1720.
(31) Zhou, T.; Zha, J. W.; Cui, R. Y.; Fan, B. H.; Yuan, J. K.; Dang, Z.-M. *ACS Appl. Mater. Interfaces* **2011**, *3*, 2184–2188.
(32) Zhao, X.; Zhao, J.; Cao, J. P.; Wang, X.; Chen, M.; Dang, Z.-M. *J. Phys. Chem. B* **2013**, *117*, 2505–2515.
(33) Lin, D. J.; Chang, C. L.; Huang, F. M.; Cheng, L. P. *Polymer* **2003**, *44*, 413–422.
(34) Moharjir, B. E.; Heymans, N. *Polymer* **2001**, *42*, 5661–5667.
(35) Choi, S.; Im, H.; Kim, J. *Nanotechnology* **2012**, *23*, 06530301–06530310.
(36) Zha, J. W.; Zhu, Y. H.; Li, W. K.; Bai, J. B.; Dang, Z. M. *Appl. Phys. Lett.* **2012**, *101*, 062905–062914.
(37) Zhou, Y.; Wang, L.; Zhang, H.; Bai, Y.; Niu, Y.; Wang, H. *Appl. Phys. Lett.* **2012**, *101*, 0129031–0129034.
(38) Wattanakul, K.; Manuspiya, H.; Yanumet, N. *J. Compos. Mater.* **2011**, *45*, 1967–1980.
(39) Agari, Y.; Ueda, A.; Tanaka, M.; Nagai, S. *J. Appl. Polym. Sci.* **1990**, *40*, 929–941.